Journal of Power Sources 222 (2013) 526–532

Contents lists available at SciVerse ScienceDirect

Journal of Power Sources

journal homepage: www.elsevier.com/locate/jpowsour

Graphene wrapped SnCo nanoparticles for high-capacity lithium ion storage

Peng Chen, Lei Guo, Yong Wang*

Department of Chemical Engineering, School of Environmental and Chemical Engineering, Shanghai University, Shangda Road 99, Shanghai 200444, PR China

HIGHLIGHTS

- Graphene-wrapped SnCo nanoparticles are prepared by a facile solution route.
- The composite shows an extremely high reversible capacity of 1117 mAh g^{-1} at 0.1C.
- It also exhibits good high-rate capability and cycling performances.

ARTICLE INFO

Article history:
Received 4 July 2012
Received in revised form
22 August 2012
Accepted 8 September 2012
Available online 13 September 2012

Keywords:
Anode materials
Graphene
Lithium ion batteries
Tin-cobalt alloy

ABSTRACT

Graphene nanosheets (GNS) wrapped SnCo alloy nanoparticles are prepared by a chemical reduction method on an ice water bath. SnCo nanoparticles are dispersed uniformly on GNS and their particle sizes are around 8-12 nm, which are substantially smaller than the pristine SnCo particles (~80-180 nm) prepared in the absence of GNS. The GNS-SnCo composite is fabricated as an anode material for lithium ion batteries. It shows a distinguished higher-than-theoretical capacity of 1117 mAh g^{-1} at 72 mA g^{-1}, which is larger than bare GNS (727 mAh g^{-1}) or Sn-Co particles (599 mAh g^{-1}). Moreover, the GNS-SnCo composite shows a good rate performance at a large current of 720 mA g^{-1}. A high capacity of 922 mAh g^{-1} is retained with more stable cycle life than that at a small current. These improved cycling performances are attributed to the complimentary effect of three elements. The mechanical stability of Sn upon cycling is improved by the presence of robust and electrically conductive GNS and the alleviated function of inactive cobalt element. The agglomeration of GNS is also hindered by the spacing effect of SnCo nanoparticles among neighboring GNS materials.

1. Introduction

Lithium ion batteries have been widely used as power sources for portable electronic devices in recent years[1-3]. As the commercial anode, graphite's theoretical capacity (372 mAh g^{-1}) is too small to meet the development of next generation lithium ion batteries. Due to its high theoretical capacity (994 mAh g^{-1}), tin-based anode has been investigated as the promising alternative to carbonaceous materials. However, the critical problem (large volume change during the Li insertion and extraction) would lead to the partial electrode pulverization and cracking[1-3]. To minimize such detrimental effect, various tin-cobalt based materials mainly including Sn-Co alloys[4-20] and Sn-Co-C composites [21-42] have recently attracted great attentions for their improved mechanical stability and electrochemical properties. As an inactive element, the cobalt element can restraint the agglomeration of nanosized tin particles and alleviate the large volume change during the Li insertion and extraction process[4-20]. Moreover, the introduction of carbonaceous materials can prevent nanoparticle agglomeration and enhance the structural stability and electrical contact of Sn-based electrode materials[21-42].

Since its discovery in 2004, graphene and its derivative composites have drawn intensive interest for abundant applications owing to their outstanding characteristics such as high electrical conductivity, strong mechanical stability, large space area, etc. [43,44]. Graphene-based materials have been investigated as active anode materials for lithium ion batteries and could exhibit a large lithium-ion storage capacity (~500-1100 mAh g^{-1})[45-49]. Being a two dimensional material, graphene has also been suggested as a promising matrix to be composited with other high-capacity electrodes materials[50-56]. To the best of our knowledge, graphene-SnCo composite is not yet to be reported in the literature.

Herein, graphene nanosheets (GNS) wrapped SnCo nanoparticles were prepared by a facile chemical reduction method on an ice water bath and their Li-ion storage properties were explored in this work. The obtained composite showed superior high lithium storage capacity and good cycling properties at both small and large currents.

* Corresponding author. Tel.: +86 21 66137723; fax: +86 21 66137725.
E-mail address: yongwang@shu.edu.cn (Y. Wang).

0378-7753/$ – see front matter © 2012 Elsevier B.V. All rights reserved.
http://dx.doi.org/10.1016/j.jpowsour.2012.09.026

2. Experimental

2.1. Preparation of graphene oxide

Graphene oxide (GO) was synthesized by a modified Hummers method [57]. 1 g natural graphite powder (Sinopharm Chemical) was dispersed in 50 ml 65 wt% HNO_3 aqueous solution (Sinopharm Chemical) and 50 ml 98 wt% H_2SO_4 aqueous solution (Sinopharm Chemical), while the temperature was maintained at ~10 °C in an ice-water bath. After magnetic stirring for 30 min, 5 g $KMnO_4$ (Sinopharm Chemical) was slowly added into the system and reacted for 2 h under magnetic stirring. Then 200 ml deionized water and 5 ml 30 wt% H_2O_2 aqueous solution (Sinopharm Chemical) were added to the solution, followed by washing with 15 ml 10 wt% HCl aqueous solution (Sinopharm Chemical). After the process of ultrasonication for 1 h, centrifuging (12000 rpm) from copious washing with deionized water and dry, the graphene oxide was obtained.

2.2. Preparation of graphene wrapped SnCo alloy particle

20 ml 0.007 M $SnCl_4 \cdot 5H_2O$ aqueous solution, 20 ml 0.007 M $CoCl_2 \cdot 6H_2O$ aqueous solution, 20 ml 0.014 M trisodium citrate acid and 20 ml 0.007 M sodium dodecyl benzene sulfonate were mixed and stirred for a few minutes to form a transparent solution. 0.12 g as-synthesized graphene oxide (GO) was ultrasonically dispersed in 20 ml deionzed water and then added to the mixed solution. 20 ml 0.01 M sodium borohydride aqueous solution was added dropwise to the reaction system and the temperature was controlled at 0-5 °C on an ice-water bath. After continuous magnetic stirring for 2 h, the precipitates (GO supported SnCo nanoparticles) were collected by centrifugation, copious washing with deionized water and drying. These GO supported SnCo nanoparticles were heated in a tube furnace in a flow of 40 sccm N_2 at 300 °C for 2 h. The graphene nanosheets (GNS) supported SnCo nanoparticles were obtained as the final product. The pristine Sn-Co alloy nanoparticles were prepared by a similar procedure except for the absence of GO materials.

2.3. Materials characterizations

The obtained products were characterized by X-ray diffraction (XRD, Rigaku D/max-2550V, Cu Kα radiation), Gas Chemisorption Analyzer(ASAP 2020, Micromeritics), field-emission scanning electron microscopy (FE-SEM, JSM-6700F) with an energy dispersive X-ray spectrometer (EDS), and transmission electron microscopy/selected area electron diffraction (TEM/SEAD, JEOL JEM-200CX and JEM-2010F) in the Instrumental Analysis and Research Center of Shanghai University. Raman spectroscopy was recorded on Renishaw in plus laser Raman spectrometer (excitation wavelength=785 nm, excitation power=3 mW, spot size=1.2 μm). Fourier transform infrared (FTIR) spectra were collected by a BIO-RAD FTS 135 FTIR spectrophotometer using the KBr pellet method. The carbon and sulfur elements were measured by a high-frequency infrared carbon-sulfur analyzer (Keguo Instrument, HCS-500P). The electrical conductivity was measured by a four-electrode method using a conductivity detection meter (Shanghai Fortune Instrument, FZ-2010).

2.4. Electrochemical measurements

The working electrodes were composed of 80 wt% of active material, 10 wt% of the conductivity agent (acetylene black), and 10 wt% of the binder (poly vinylidene difluoride, PVDF, Aldrich). Lithium foil (China Energy Lithium Co., Ltd) was used as counter

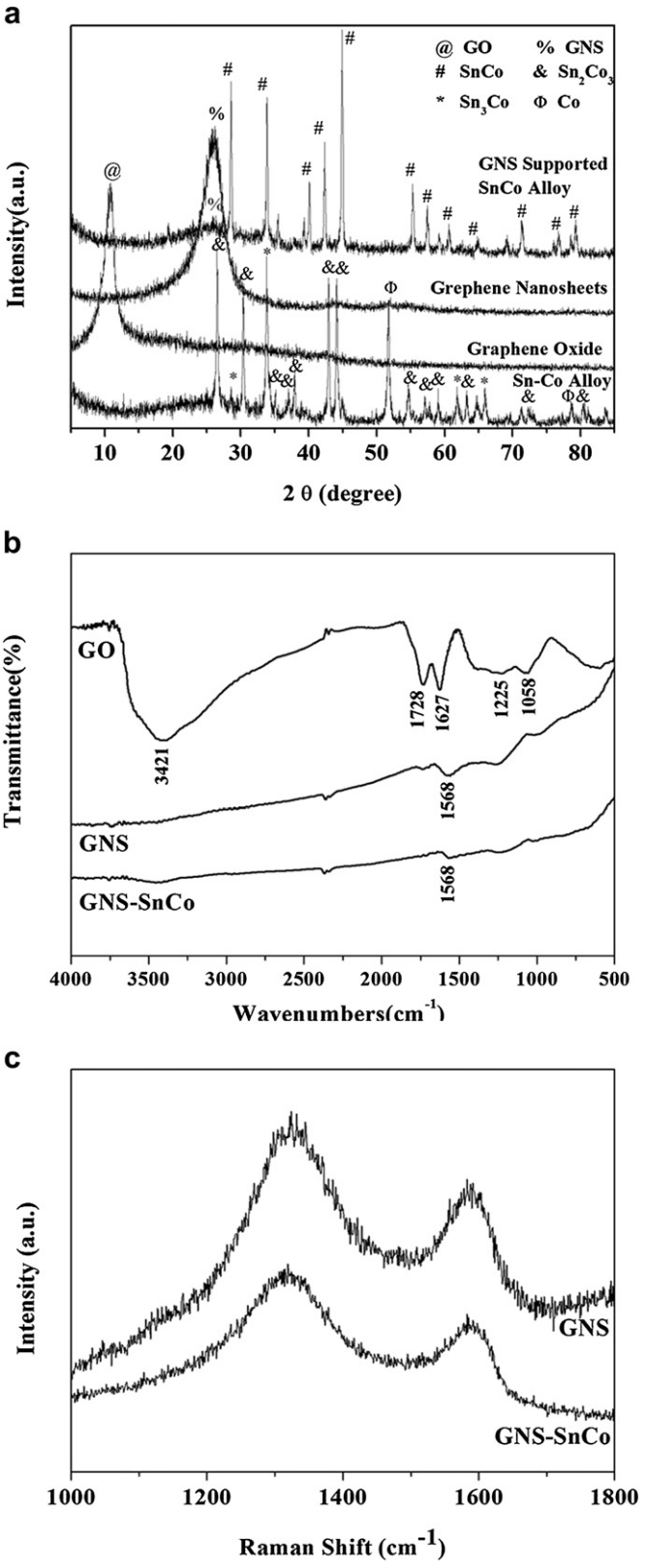

Fig. 1. (a) XRD patterns of graphene oxide (GO), graphene nanosheets(GNS), Sn-Co alloy particles and GNS wrapped SnCo nanoparticles (GNS-SnCo). (b) FTIR spectra of GO, GNS and GNS-SnCo. (c) Raman spectra of GNS and GNS-SnCo.

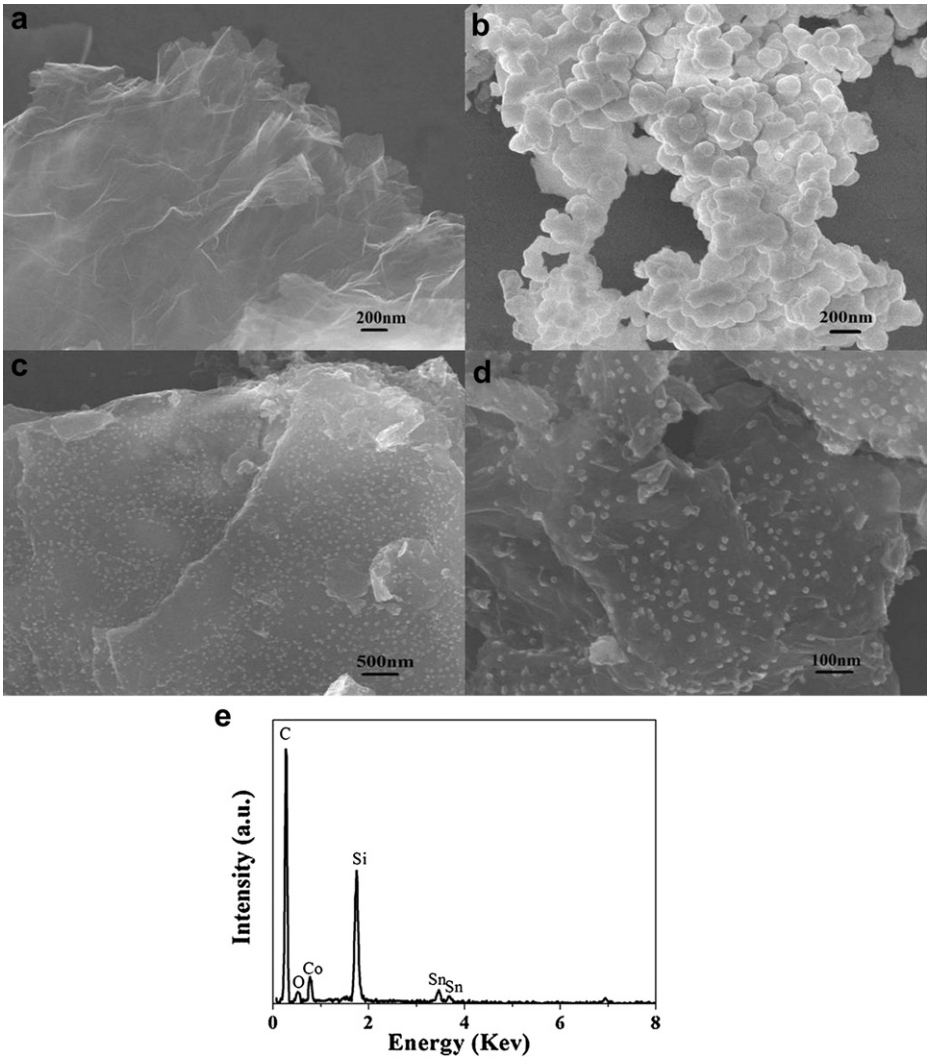

Fig. 2. SEM images of (a) GNS, (b) Sn-Co alloy particles, (c,d) GNS wrapped SnCo nanoparticles. (e) the EDS pattern of GNS wrapped SnCo nanoparticles.

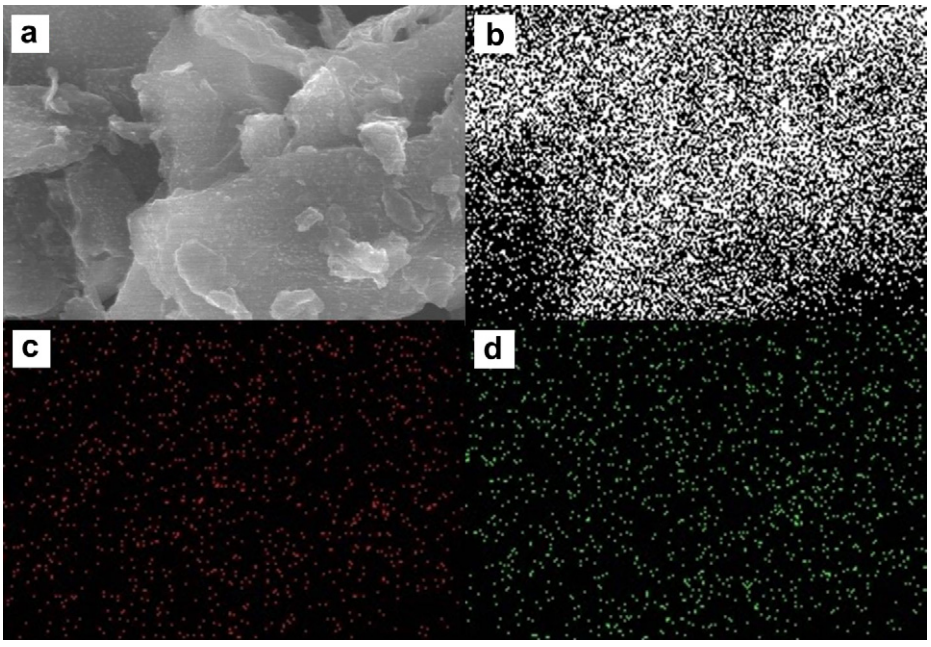

Fig. 3. EDS element mapping of GNS wrapped SnCo nanoparticles: (a) SEM image. EDS element mapping images of (b) C, (c) Sn, (d) Co elements.

and reference electrode. The electrolyte was 1 M $LiPF_6$ in a 50:50 w/w mixture of ethylene carbonate (EC) and diethyl carbonate (DEC). Electrochemical measurements were performed on a LAND-CT2100C test system at a constant temperature of 25 °C. The Swagelok-type cells were discharged and charged at a constant current (72 mA g^{-1}, 0.1 C, 1 C=720 mA g^{-1}) in the fixed voltage range 5 mV -3 V. The loading amount of the electrode was kept at ~2 mg cm^{-2}. A high rate of 1 C was also used and the first cycle discharging was kept at 0.1 C.

3. Results and discussion

The XRD patterns of GO, GNS, Sn-Co particles and GNS wrapped SnCo nanoparticles are shown in Figure 1a. There was a characteristic peak of GO at 10.8°, indicating that the interplanar spacing was around 0.818 nm. After the thermal reduction, this peak was shifted to 25.7°. The corresponding interplanar spacing of GNS was 0.346 nm, which was slightly larger than that of standard graphite (0.335 nm). For the XRD patterns of Sn-Co alloy nanoparticles, a few characteristic peaks could be observed, which could be ascribed to a mixed phase of Sn_2Co_3 (PDF 26-0490), Sn_3Co (PDF 48-1813) and Co (PDF 15-0806). However, in the presence of GNS, a few characteristic peaks were readily indexed to a pristine phase of SnCo (PDF 02-0559). There were no more peaks corresponding to other Sn-Co alloys and Co metal.

The FTIR spectra of GO, GNS and GNS-SnCo composite are shown in Figure 1b. The peak at 3421 cm^{-1} of GO was attributed to the O-H stretching vibration of adsorbed water molecules and surface OH groups. A few stretches of 1728 and 1225 cm^{-1} could be attributed to the presence of abundant O=C and O-C functional groups on the GO surface. It is suggested that these surface groups of GNS may hinder the particle growth of Sn-Co particles in the preparation process. After a thermal reduction, these oxygen-containing functional groups in GNS-SnCo composite were not found, confirming that GO had been reduced to GNS. For GNS and GNS-SnCo composite, a small stretch appeared at 1568 cm^{-1}, which could be ascribed to the skeletal vibration of graphene sheets [49].

The Raman spectra of GNS and GNS-SnCo composite are shown in Figure 1c. Two characteristic peaks of the D and G bands from GNS were observed at 1330 and 1580 cm^{-1}. The intensity ratios of D and G band (I_D: I_G) were 1.21 and 1.28 for GNS and GNS-SnCo composite respectively. The more disordered carbon structure in the GNS-SnCo composite compared with bare GNS may be due to the partial insertion of SnCo particles into GNS. This disordered structure may be beneficial to the enhanced lithium-ion storage capacity and faciliated lithium diffusion through graphene layers.

FESEM images in Figure 2a-d show the surface morphologies of GNS, Sn-Co particles and GNS wrapped SnCo nanoparticles. GNS could be observed as several layers stacking of single graphene nanosheet (Figure 2a). Pristine Sn-Co alloys with particle morphology were found with particle sizes around 80-180 nm (Figure 2b). When GNS were added in the preparation process, SnCo nanoparticles were obtained with substantially smaller particle sizes of ~8-12 nm. These nanoparticles were dispersed uniformly on GNS surface and there was no detectable particle agglomeration as shown in Figure 2c-d. The energy dispersive X-ray spectroscopy (EDS) results of GNS-SnCo composite are shown in Figure 2e. A few elements such as C, O, Sn and Co were present in the composite. The Si element was observed because Si substrate was used to disperse GNS-SnCo sample for SEM measurment, thus removing the carbon effect from the commonly used substrate of carbon paste. The composite was also measured by a high-frequent infrared carbon analyzer. The elemental analysis of C in the composites revealed that the carbon content was 82.2% in GNS-SnCo composite. This value is slightly larger than the theoretical value (75 wt% carbon) based on the experimental calculation. The molar ratio of Sn:Co was estimated to be 1:1 in the composite by the energy dispersive spectra (EDS) results. The BET surface area of the composite was measured to be ~176.2 m^2 g^{-1}.

Figure 3a shows a typical SEM image of the GNS-SnCo composite, along with the corresponding C (Figure 3b), Sn (Figure 3c), Co (Figure 3d) mapping images. These evenly-distributed points of Sn, Co and C elements confirmed the uniform dispersion of SnCo particles on the GNS. These small

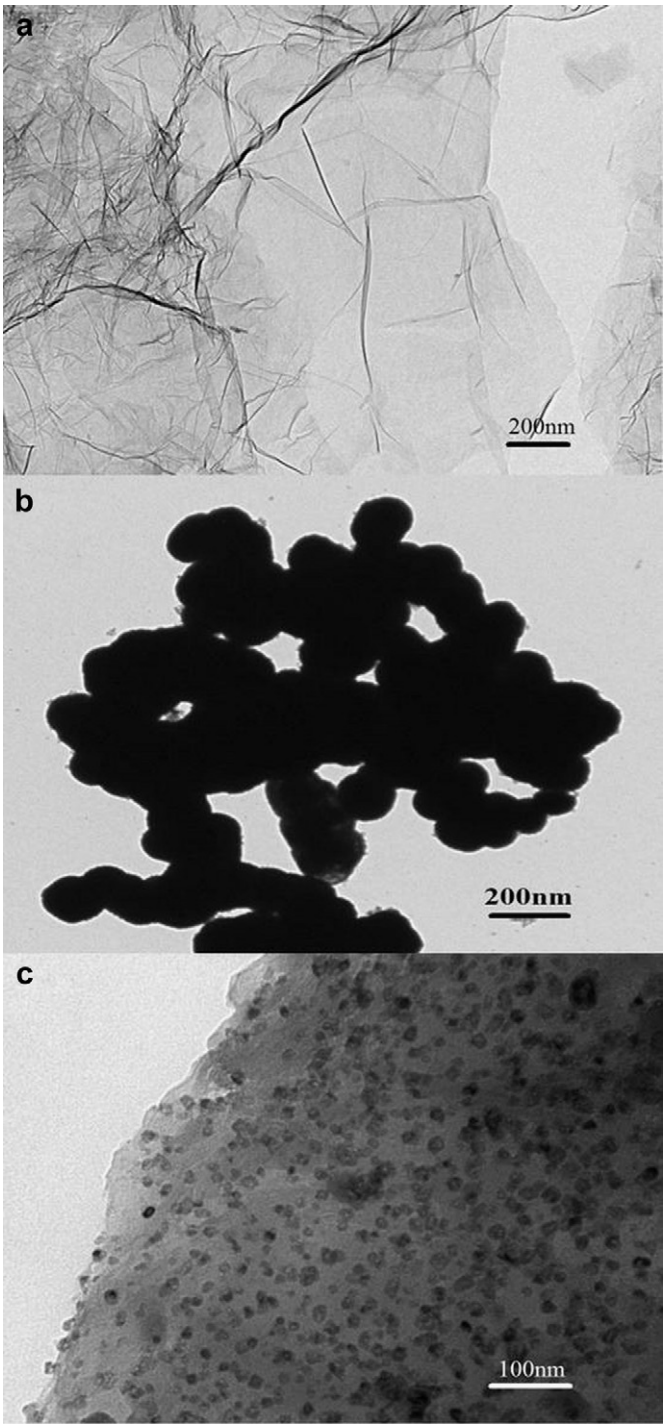

Fig. 4. TEM images of (a) GNS, (b) Sn-Co alloy particles, (c) GNS wrapped SnCo nanoparticles.

particle size and narrow particle size distribution of SnCo materials on GNS are highly desirable when used as anode materials for lithium ion batteries because uniform and small local volume change would be caused upon cycling[1-3], which should be easier to be relieved by GNS material. Figures 4a-c show TEM images of GNS, Sn-Co particles and GNS wrapped SnCo nanoparticles. GNS were quite thin under the electron imaging (Figure 4a). Pristine Sn-Co alloy particles were around 80-180 nm and contacted with each other in Figure 4b. A large number of SnCo nanoparticles were found on GNS as shown in Figure 4c. These nanoparticles were quite uniformly dispersed without detectable particle agglomeration. It should be attributed to the binding effect of GNS, which limits the particle movement and agglomeration. A schematic sketch of the growth process of GNS wrapped SnCo nanoparticles is shown in Figure 5. SnCo nanoparticles were wrapped by GNS and formed a sandwiched composite nanostructure. The agglomeration of GNS should be hindered in the composite due to the presence of a number of SnCo particles. These nanoparticles are located within GNS stacking and can prevent their contact to some extent.

Sn-Co based materials have been suggested as promising anodes for lithium ion batteries. Various carbon supported Sn-Co composites have been investigated[21-42]. It should be also meaningful to explore the effect of graphene matrix when composited with SnCo materials. The electrochemical performances of Sn-Co alloy, GNS and GNS wrapped SnCo nanoparticles at a constant small current of 72 mA g^{-1} (0.1C, 1C= 720 mA g^{-1}) are compared in Fig. 6a-b. There are two plateaus in the discharge curve of pure Sn-Co alloy. The voltage plateau at ~1.0-1.2 V should be ascribed to the decomposition of electrolyte and the formation of a solid electrolyte interphase (SEI) film or the reduction of impure metal oxides on Sn-Co alloy surface [20,38]. Another plateau (~0.4-0.5V) can be ascribed to the lithiation reaction of Sn and subsequently the formation of Li_xSn alloy[2]. The reversible delithiation process can be also indicated by the plateau (~0.5-0.8V) in the corresponding charge curve. In comparison, these plateaus due to the lithiation and delithiation process of Sn are not very clear for the graphene/Sn-Co composite because there is a large amount of 82.2% graphene in the composite. Pristine graphene exhibits a plateau around 0.75 V, which is readily ascribed to the formation of SEI film on graphene[46]. The initial charge capacity (lithium extraction) of GNS wrapped SnCo nanoparticles was 1117 mAh g^{-1}, which was substantially higher than those of GNS (727 mAh g^{-1}) and Sn-Co alloy (599 mAh g^{-1}). To our knowledge, this large reversible capacity (1117 mAh g^{-1}) is not witnessed in all previous Sn-Co and Sn-Co-C composites anodes. Although the mechanism for extremely high capacity is not very clear, it is believed that the extra amount of lithium ion may be mainly due to the more disordered carbon structure, which is partially proved by the Raman spectra results of GNS and GNS-SnCo composite (Fig. 1c). The expanded (002) interlayer spacing in disordered GNS has been suggested for enhancing the Li-ion storage capacity [45]. Lithium ions can also be stored in micro-voids surrounded by hexagonal planes and cluster gap between edges of carbon hexagon clusters caused by the insertion of SnCo nanoparticles into GNS layers[58]. The Li-ion storage has also been suggested by a possible faradaic capacitance [49] and absorption on both sides of graphene [45,46]. Initial discharge capacities (lithium insertion) were 1409 mAh g^{-1} and 1125 mAh g^{-1} for GNS and Sn-Co alloy respectively. GNS wrapped SnCo nanoparticles showed a higher initial discharge value of 1735 mAh g^{-1}. The corresponding initial Coulombic efficiencies were 51.6% and 53.2% for GNS and Sn-Co alloy respectively. The Coulombic efficiency was increased to 64.4% for GNS wrapped SnCo nanoparticles. The large initial capacity loss should be mainly ascribed to the lithium ion consumption in the electrolyte decomposition and the formation of solid electrolyte interface (SEI) film around the GNS/SnCo electrode with a large surface area of 176.2 m^2 g^{-1}. This shortcoming was reported for almost all nanoscaled electrodes due to their large surface areas and could be improved by the material pretreatment such as pre-lithiation [3].

The cycling performances of Sn-Co alloy, GNS and GNS wrapped SnCo nanoparticles (17.8 wt% SnCo) at 0.1 C are shown in the Fig. 6b. In general, there were fast capacity fadings for three types of electrodes during the initial 20 cycles, however the cycliability became stable during the following 20-60 cycles. The charge capacity of GNS wrapped SnCo nanoparticles was 571 mAh g^{-1} after 60 cycles, which was higher than those of GNS (324 mAh g^{-1}) and Sn-Co alloy (210 mAh g^{-1}) after the same cycles. This value (571 mAh g^{-1}) is also larger than commercial graphite supported Sn-Co nanoparticles (~400 mAh g^{-1})[22,23] and most previous Sn-Co-C reports[24-38] after similar cycle numbers. The achieved reversible capacities (1117 -571 mAh g^{-1}) in 60 cycles are also comparable to previous transitional metal oxides or tin-based anodes[50-56]. Fig. 6c shows the contribution of SnCo alloy or

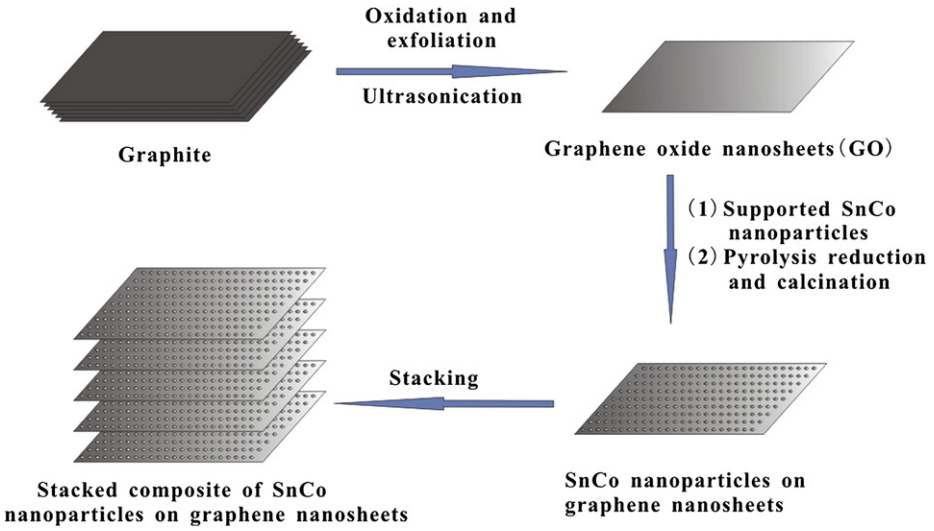

Fig. 5. Schematic illustration of the formation process of GNS wrapped SnCo nanoparticles.

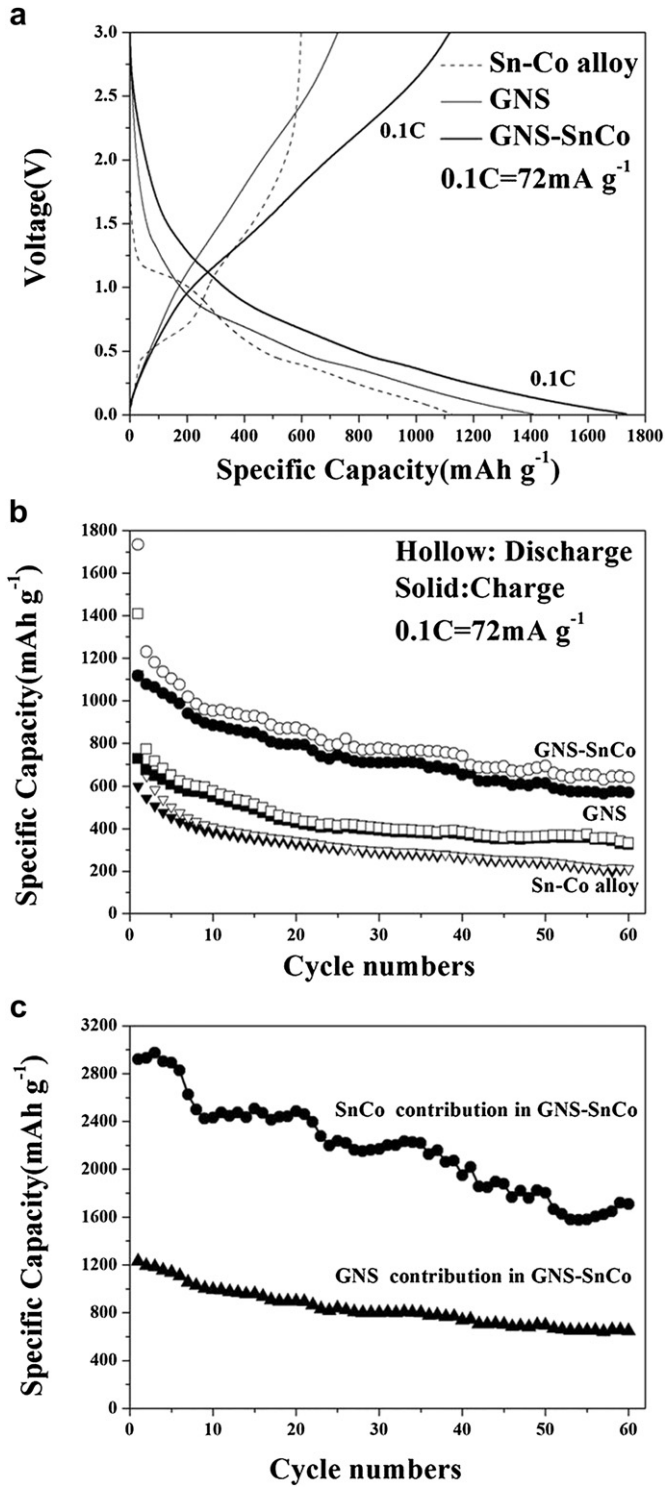

Fig. 6. (a) First-cycle discharge (lithium insertion) and charge (lithium extraction) curves of the products at 0.1 C. (b) Cycling performances of the products at 0.1 C. (C) the capacity contribution of SnCo and GNS in the composite, assuming the other one has no capacity improvement in the composite.

GNS assuming the other one contributes no capacity improvement in the composite. Very large capacity contribution could be observed for both SnCo and GNS materials, indicating a distinguished synergetic effect in the composite for the enhanced Li-ion storage capacity. These improved electrochemical performances should be largely attributed to the usage of robust, flexible and electrically conductive GNS. The volume expansion of Sn during the electrochemical cycles could be buffered or relieved to some extent by flexible GNS wrapping. The electrical contact of Sn particles is also improved by high electrically conductive GNS. As measured by a four-electrode method, GNS-SnCo composite exhibits an electrical conductivity of 5.23 s cm^{-1}, which is higher than Sn-Co alloy (2.25 s cm^{-1}). The Co element also increases further the mechanical stability upon repetitive cycling with lithium ions[4-20]. It is suggested that if SnCo nanoparticles are further coated by a carbon overlayer[51], better cycling stability may be achieved.

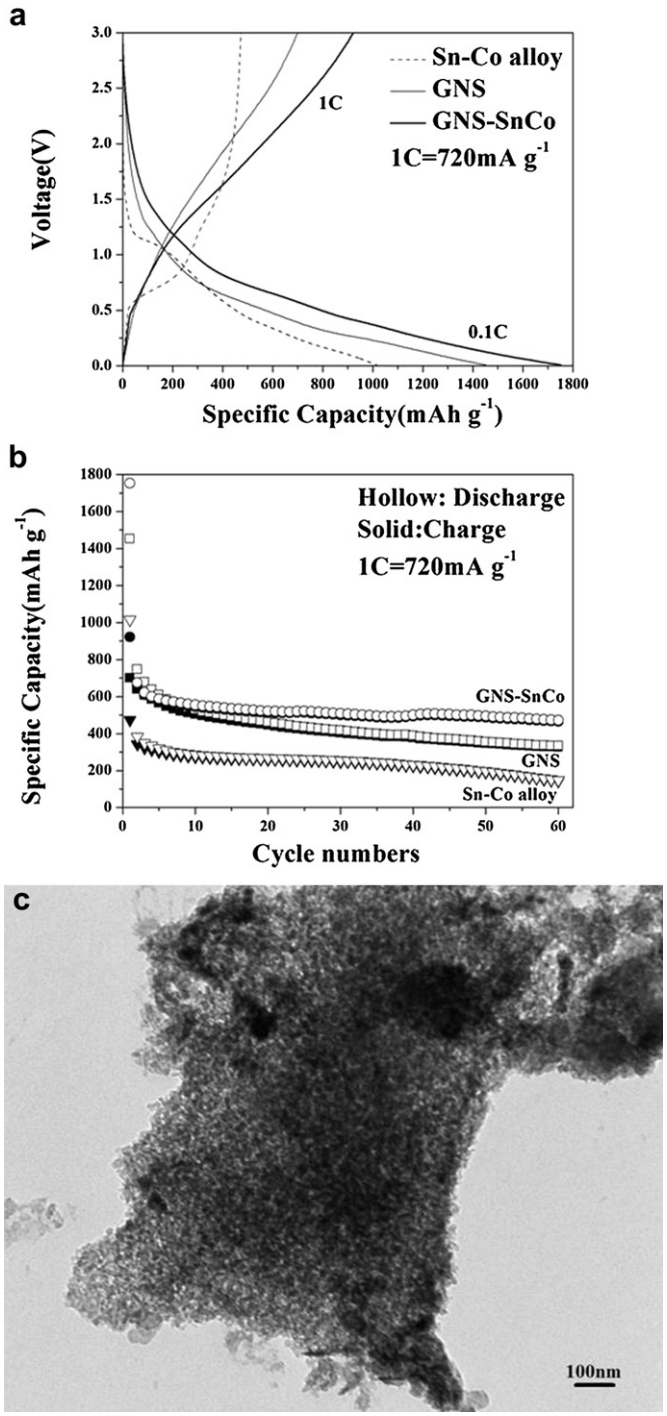

Fig. 7. (a) First-cycle discharge (lithium insertion) and charge (lithium extraction) curves of the products at 1 C. (b) Cycling performances of the products at 1 C. (c) TEM image of GNS wrapped SnCo nanoparticles after cycling.

The high-rate electrochemical performances of Sn-Co alloy, GNS and GNS wrapped SnCo nanoparticles were also explored as shown in the Fig. 7a-b. In comparison, the initial charge capacities of Sn-Co alloy, GNS and GNS wrapped SnCo nanoparticles were 473 mAh g^{-1}, 700 mAh g^{-1} and 922 mAh g^{-1} respectively at a high rate of 1 C (720 mA g^{-1}). These values were all lower than the corresponding capacities at 0.1 C. However, three composites exhibited more stable cycle life compared to their performances at 0.1 C. It may be because those extra amount of lithium ions at a smaller current are more inclined to be trapped in the "bad" pores or microcavities of the electrode materials. However, most inserted lithium ions at a fast current are stored in comparatively "good" places, in which lithium ions can be easily stored and exhibit a good reversibility. As a result, a more stable cycliability would be achieved at a large current. A similar better high-rate cycliability was also observed in the GNS-CuO composite anodes[56]. The TEM image of GNS-SnCo composite after cycling is shown in Figure 7c. The conductive agent (carbon black) and binder materials (PVDF) were also present in the cycled electrode materials. There was no detection of large agglomerated SnCo particles in this image and it is believed that most SnCo nanoparticles were protected well by GNS wrapping against their agglomeration upon repetitive cycling with lithium ions.

4. Conclusion

In summary, the composite of GNS wrapped SnCo alloy nanoparticles was prepared by a chemical reduction method on an ice water bath and its lithium ion storage properties were explored. It showed an extremely large reversible capacity of 1117 mAh g^{-1} at a small current of 72 mA g^{-1} and 922 mAh g^{-1} at a large current of 720 mA g^{-1} in the first cycle. These high capacities at both small and large currents were not witnessed in previous Sn-Co-C relative literature. Moreover, in spite of comparatively faster capacity fading in the initial several cycles, good cycliabilities were achieved during prolonged cycles, especially at a large test current. These improved electrochemical properties have been ascribed to the complimentary effect of three components (Sn, Co, GNS), where good electrical contact, strong mechanical stability, and promoted lithium diffusion and storage could be preserved in the repetitive cycling with lithium ions.

Acknowledgements

The authors gratefully acknowledge the Professor of Special Appointment (Eastern Scholar) in Shanghai, the National Natural Science Foundation of China (51271105), Shanghai Municipal Government (11JC1403900, 11SG38, S30109) for financial support.

References

[1] Z.Y. Zhou, N. Tian, J.T. Li, I. Broadwell, S.G. Sun, Chem. Soc. Rev. 40 (2011) 4167–4185.
[2] C.M. Park, J.H. Kim, H. Kim, H.J. Sohn, Chem. Soc. Rev. 39 (2010) 3115–3141.
[3] P. Verma, P. Maire, P. Novak, Electrochim. Acta 55 (2010) 6332–6341.
[4] L.J. Xue, Y.F. Xu, L. Huang, F.S. Ke, Y. He, Y.X. Wang, G.Z. Wei, J.T. Li, S.G. Sun, Electrochim. Acta 56 (2011) 5979–5987.
[5] H. Groult, H. EI Ghallali, A. Barhoun, E. Briot, C.M. Julien, F. Lantelme, S. Borensztjan, Electrochim. Acta 56 (2011) 2656–2664.
[6] C.G. Yang, D.W. Zhang, Y.B. Zhao, Y.H. Lu, L. Wang, J.B. Goodenough, J. Power Sources 196 (2011) 10673–10678.
[7] X.Y. Fan, F.S. Ke, G.Z. Wei, L. Huang, S.G. Sun, J. Solid State Electrochem 13 (2009) 1849–1858.
[8] J.T. Li, S.R. Chen, F.S. Ke, G.Z. Wei, L. Huang, S.G. Sun, J. Electroanal. Chem. 649 (2010) 171–176.
[9] H. Guo, H.L. Zhao, X.D. Jia, X. Li, W.H. Qiu, Electrochim. Acta 52 (2007) 4853–4857.
[10] H. Kim, J. Cho, Electrochim. Acta 52 (2007) 4197–4201.
[11] P.A. Connor, J.T.S. Irvine, Electrochim. Acta 47 (2002) 2885–2892.
[12] M. Valvo, U. Lafont, L. Simonin, E.M. Kelder, J. Power Sources 174 (2007) 428–434.
[13] G. Ferrara, L. Damen, C. Arbizzani, R. Inguanta, S. Piazza, C. Sunseri, M. Mastragostino, J. Power Sources 196 (2011) 1469–1473.
[14] J.T. Li, J. Swiatowska, A. Seyeux, L. Huang, V. Maurice, S.G. Sun, P. Marcus, J. Power Sources 195 (2010) 8251–8257.
[15] K. Ui, S. Kikuchi, Y. Jimba, N. Kumagai, J. Power Sources 196 (2011) 3916–3920.
[16] F.S. Ke, L. Huang, H.B. Wei, J.S. Cai, X.Y. Fan, F.Z. Yang, S.G. Sun, J. Power Sources 170 (2007) 450–455.
[17] X.Y. Fan, F.S. Ke, G.Z. Wei, L. Huang, S.G. Sun, J. Alloys Compd 476 (2009) 70–73.
[18] F. Nacimiento, R. Alcantara, J.L. Tirado, J. Alloys Compd 485 (2009) 385–390.
[19] X.J. Zhu, Z.P. Guo, P. Zhang, G.D. Du, R. Zeng, Z.X. Chen, S. Li, H.K. Liu, J. Mater. Chem. 19 (2009) 8360–8365.
[20] Z.J. Du, S.C. Zhang, J. Phys. Chem. C 115 (2011) 23603–23609.
[21] A.D.W. Todd, R.E. Mar, J.R. Dahn, J. Electrochem. Soc 154 (2007) A597–A604.
[22] Q. Fan, P.J. Chufas, M.S. Whittingham, Electrochem. Solid-State Lett. 10 (2007) A274–A278.
[23] R. Zhang, M.S. Whittingham, Electrochem. Solid-State Lett. 13 (2010) A184–A187.
[24] P.P. Ferguson, M.L. Martine, R.A. Dunlap, J.R. Dahn, Electrochim. Acta 54 (2009) 4534–4539.
[25] T. Huang, Y. Yao, Z. Wei, Z. Liu, A. Yu, Electrochim. Acta 56 (2010) 476–482.
[26] J. Li, D.B. Le, P.P. Ferguson, J.R. Dahn, Electrochim. Acta 55 (2010) 2991–2995.
[27] J. Hassoun, P. Ochal, S. Panero, G. Mulas, C.B. Minella, B. Scrosati, J. Power Sources 180 (2008) 568–575.
[28] P.P. Ferguson, M.L. Martine, A.E. George, J.R. Dahn, J. Power Sources 194 (2009) 794–800.
[29] J. Hassoun, S. Panero, G. Mulas, B. Scrosati, J. Power Sources 171 (2007) 928–931.
[30] G.F. Ortiz, R. Alcantara, I. Rodriguez, J.L. Tirado, J. Electroanal. Chem. 605 (2007) 98–108.
[31] J. Hassoun, G. Mulas, S. Panero, B. Scrosati, Electrochem. Common 9 (2007) 2075–2081.
[32] R.B. Lewis, A. Timmons, R.E. Mar, J.R. Dahn, J. Electrochem. Soc. 154 (2007) A213–A216.
[33] P. Lavela, F. Nacimiento, G.F. Ortiz, J.L. Tirado, J. Solid State Electrochem 14 (2010) 139–148.
[34] Z.X. Chen, J.F. Qian, X.P. Ai, Y.L. Cao, H.X. Yang, J. Power Sources 189 (2009) 730–732.
[35] S.I. Lee, S. Yoon, C.M. Park, J.M. Lee, H. Kim, D. Im, S.G. Doo, H.J. Sohn, Electrochim. Acta 54 (2008) 364–369.
[36] J.C. He, H.L. Zhao, M.W. Wang, X.D. Jia, Mater. Sci. Eng., B 171 (2010) 35–39.
[37] W.J. Cui, F. Wang, J. Wang, C.X. Wang, Y.Y. Xia, Electrochim. Acta 56 (2011) 4812–4818.
[38] L. Huang, J.S. Cai, Y. He, F.S. Ke, S.G. Sun, Electrochem. Commun 11 (2009) 950–953.
[39] P.P. Ferguson, A.D.W. Todd, J.R. Dahn, Electrochem. Commun 10 (2008) 25–31.
[40] P.P. Ferguson, A.D.W. Todd, J.R. Dahn, Electrochem. Commun 12 (2010) 1041–1044.
[41] M.Y. Li, C.L. Liu, M.R. Shi, W.S. Dong, Electrochim. Acta 56 (2010) 3023–3028.
[42] A.D.W. Todd, R.A. Dunlap, J.R. Dahn, J. Alloys Compd 443 (2007) 114–120.
[43] K.S. Novoselov, A.K. Geim, S.V. Morozov, D. Jiang, Y. Zhang, S.V. Dubonos, I.V. Grigorieva, A.A. Firsov, Science 306 (2004) 666–669.
[44] A.K. Geim, K.S. Novoselov, Nat. Mater 6 (2007) 183–191.
[45] E.J. Yoo, J. Kim, E. Hosono, H.S. Zhou, T. Kudo, I. Honma, Nano Lett. 8 (2008) 2277–2282.
[46] P. Guo, H.H. Song, X.H. Chen, Electrochem. Commun 11 (2009) 1320–1324.
[47] C.Y. Wang, D. Li, C.O. Too, G.G. Wallace, Chem. Mater 21 (2009) 2604–2606.
[48] G.X. Wang, X.P. Shen, J. Yao, J. Park, Carbon 47 (2009) 2049–2053.
[49] A.V. Murugan, T. Muraliganth, A. Manthiram, Chem. Mater 21 (2009) 5004–5006.
[50] S.Q. Chen, Y. Wang, J. Mater. Chem. 20 (2010) 9735–9739.
[51] S.Q. Chen, P. Chen, M.H. Wu, D.Y. Pan, Y. Wang, Electrochem. Commun 12 (2010) 1302–1306.
[52] Y.Q. Zou, Y. Wang, Nanoscale 3 (2011) 2615–2620.
[53] Y.Q. Zou, Y. Wang, ACS Nano 5 (2011) 8108–8114.
[54] Y.Q. Zou, J. Kan, Y. Wang, J. Phys, Chem. C 115 (2011) 20747–20753.
[55] L.Q. Lu, Y. Wang, J. Mater. Chem. 21 (2011) 17916–17921.
[56] L.Q. Lu, Y. Wang, Electrochem. Commun 14 (2012) 82–85.
[57] W.S. Hummers, R.E. Offeman, J. Am. Chem. Soc. 80 (1958) 1339.
[58] N.A. Kaskhedikar, J. Maier, Adv. Mater 21 (2009) 2664–2680.